RESEARCH ARTICLE

# Ceramic foam substrates for automotive catalyst applications: fluid mechanic analysis

Panayotis Dimopoulos Eggenschwiler ·
Dimitrios N. Tsinoglou · Jacqueline Seyfert ·
Christian Bach · Ulrich Vogt · Michal Gorbar

**Abstract** Several properties of ceramic foams render them promising substrates for various industrial processes. For automotive applications, the foam properties that need to be further studied include the substrate impact on the exhaust gas flow, in terms of pressure drop and flow uniformity. In this paper, pressure drop measurements are performed with different honeycomb and ceramic foam substrates, and pressure drop correlations are discussed. The flow uniformity upstream and downstream of the substrates is evaluated using particle image velocimetry. The results show that ceramic foam substrates induce higher pressure drop, while increasing the uniformity of the flow. In contrast to honeycomb monoliths, the flow uniformity downstream of ceramic foams does not decrease with increasing flow velocity. The higher flow uniformity of ceramic foams is not only caused by their higher pressure drop, but also by flow homogenization that occurs inside the ceramic foam structure, as a result of the momentum exchange perpendicular to the main flow direction.

**List of symbols**

| | |
|---|---|
| $a_0, a_1$ | Pressure drop coefficients |
| $c_F$ | Form drag coefficient [–] |
| $C$ | Form drag coefficient [m$^{-1}$] |
| $d_h$ | Channel hydraulic diameter [m] |
| $d_p$ | Mean diameter of a particle in an equivalent packed bed [m] |
| $d_s$ | Diameter of the ceramic foam struts [m] |
| $E_1, E_2$ | Pressure drop coefficients |
| $K$ | Permeability [m$^2$] |
| $u$ | Local gas velocity [m/s] |
| $\bar{u}$ | Average velocity of a flow profile [m/s] |
| UF | Uniformity factor [–] |
| $a$ | Mean diameter of the ceramic foam pores [m] |
| $\Delta p/L$ | Pressure drop per unit length [Pa/m] |
| $\varepsilon$ | Porosity [–] |
| $\mu$ | Exhaust gas viscosity [Pa s] |
| $\rho$ | density [kg/m$^3$] |

P. Dimopoulos Eggenschwiler (✉) · D. N. Tsinoglou ·
J. Seyfert · C. Bach
Laboratory for I.C. Engines, Empa, Swiss Federal Laboratories
for Materials Testing and Research, Ueberlandstr. 129,
8600 Duebendorf, Switzerland
e-mail: panayotis.dimopoulos@empa.ch
URL: http://www.empa.ch

U. Vogt · M. Gorbar
Laboratory for Hydrogen Energy, Empa,
Swiss Federal Laboratories for Materials Testing and Research,
Duebendorf, Switzerland

## 1 Introduction

Ceramic foams can be applied as catalyst substrates for various industrial applications, with several advantages over conventional pellet substrates (Twigg and Richardson 2002). In the field of automotive exhaust catalysts, foam-type substrates have been proposed as alternatives to the well-established honeycomb substrates. These applications involve the use of foams as diesel particulate filters (DPF) or combined diesel oxidation catalysts (DOC), and DPF systems (Koltsakis et al. 2006; Hossfeld and Ranalli 2006; Koltsakis et al. 2008). Initial investigations of the application of ceramic foams as substrates for three-way catalytic converters (TWC) for natural gas engines have

been performed in our laboratory. The results showed similar chemical activity of ceramic foams and honeycomb monoliths at varying air-to-fuel ratios (Dimopoulos et al. 2008). Moreover, the pollutant conversion achieved with ceramic foam substrates during engine tests at representative operating points was at least as high as the one achieved with a conventional honeycomb monolith (Dimopoulos and Bach 2008). However, the pressure drop of the ceramic foam catalysts was higher compared to the honeycomb monoliths. Further developments both of the substrate material and of its integration in the exhaust system require detailed understanding of various properties of the ceramic foam substrates, compared to honeycomb substrates. These properties include mechanical properties, heat and mass transfer, washcoat pore diffusion and chemical reactions, as well as fluid dynamic properties. From the fluid dynamics point of view, the properties that need to be investigated are the pressure drop of the substrate, as well as the effect of the substrate on exhaust flow uniformity.

Pressure drop is an important property of catalytic substrates, as it affects the engine fuel consumption. The pressure drop per unit length of ceramic foams is known to be higher, compared to honeycomb monoliths. This, however, can be partly compensated, either by downsizing the ceramic foam substrate, which is made possible by the increased mass transfer of foams compared to honeycomb monoliths (Giani et al. 2005), or by using radial-flow foam substrates (Koltsakis et al. 2008), which involve smaller length for the same substrate volume.

Exhaust flow uniformity in catalytic converters plays an important role, particularly under high exhaust gas velocities. Several studies report that flow non-uniformity has a negative impact on pollutant conversion efficiency and on catalyst durability (Chakravarthy et al. 2003; Gaiser et al. 2003; Nagel and Diringer 2000; Martin et al. 1998; Zygourakis 1989). In modern exhaust aftertreatment systems, where different exhaust aftertreatment devices are used in a cascade configuration, the flow uniformity downstream of each substrate affects the performance of aftertreatment devices located further downstream. Such is the case of DPF, which are typically located directly downstream of DOC. The flow uniformity at the DPF entrance is expected to strongly affect the soot deposition uniformity. Ranalli et al. (2002) identified uniform soot deposition as a key factor for a reliable DPF system. Stratakis and Stamatelos (2004) performed hot film anemometry measurements with loaded and unloaded DPFs, and reported substantial flow non–uniformities. As a means to achieve uniform flow distribution upstream of DPFs the use of helical-type flow elements is proposed (Gaiser et al. 2003; Oesterle et al. 2004). Similar mixing devices have also been proposed to achieve uniform flow distribution

and proper mixing upstream of selective catalytic reduction (SCR) catalysts (Kaiser and Rusch 2007), where a small amount of liquid urea is injected in the exhaust line to help the reduction of nitrogen oxides. Initial investigations on the potential of achieving uniform flow distribution upstream of DPFs and SCR catalysts by using foam substrates upstream of these devices have already been performed (Dimopoulos et al. 2007).

In the present paper, we examine the performance of ceramic foam substrates with different pore densities, in terms of pressure drop and uniformity of the flow field upstream and downstream of the substrate. Correlations for the prediction of pressure drop proposed in the literature are reviewed and adapted in order to correctly predict the pressure drop across the substrates tested. Flow field measurements are performed on a cold-flow test rig, using particle image velocimetry (PIV). Compared to the more commonly applied intrusive measurement techniques, PIV has a relatively fine spatial resolution, and at the same time captures a broad area of the flow field. These properties help reveal some aspects of the flow field, which cannot be captured either by other measurement techniques, or by computational fluid dynamics (CFD) simulations, which typically treat the catalyst substrate as a continuum porous medium. Moreover, the paper discusses the correlation between the increase in pressure drop and the uniformity of the flow distribution.

## 2 Experimental set-up

### 2.1 Test flow rig

A specifically designed test flow rig has been employed with geometrical features typical for passenger car and light truck exhaust configurations. The flow medium was air, drawn off the facilities' pressure circuit, at 7 bar feed pressure. Upstream of the measurement section, the installation included a pressure reduction station, mass flow metering, and a 400-lt oscillation and noise dampener. For the mass flow measurement, a hot-film anemometer, Type ABB Sensyflow P was used. The set-up allowed stable metering of flows among 10 and 500 kg/h (Reynolds numbers between 2,000 and 100,000). Flow field measurements have been performed at six air mass flow rates, 100, 150, 200, 250, 300, and 370 kg/h. These mass flow rates have been considered typical for automotive exhaust gas flows.

The measurement section of the test flow rig has a modular design consisting of the inflow and outflow parts and the main duct with two optical access areas as well as the substrate placement area as shown in Fig. 1. The inflow part can easily be changed, allowing the assessment of
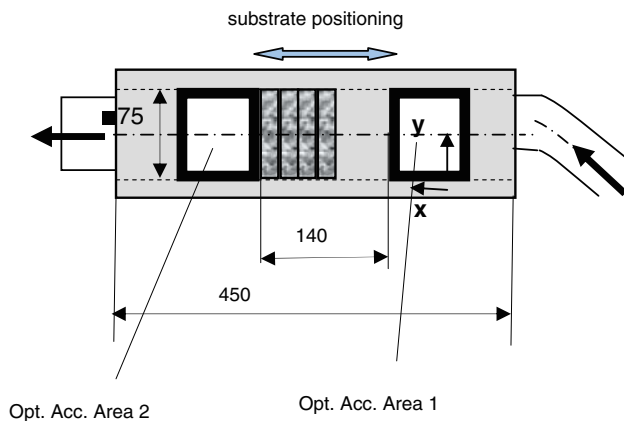
various automotive exhaust type configurations. The results and analysis presented in this work concern one inflow configuration, consisting of a 56-mm diameter inflow tube with a 45° inclination in respect to the main duct. In addition, the inflow tube axis was displaced horizontally by 10 mm to the right-hand side (flow bound observation) with reference to the main duct axis, Fig. 1. By entering the main duct, the flow undergoes a sudden expansion to an 85-mm diameter cross section. The following main duct is such that after mounting the substrates with the necessary sealing mat (3 M Interam™ 100HD) the flow cross section is square with 75 mm side-by-side dimensions (Fig. 1). The configuration chosen is typical for automotive applications introducing modest inhomogeneity levels. While the tortuous automotive underfloor imposes in many cases much sharper bends and edges we, chose this configuration for assessing the impact of the different substrates on modest inhomogeneity levels. The optical access areas consist of a detachable quartz glass window on all sides. For a more detailed description of the test flow rig the interested reader is referred to (Dimopoulos et al. 2007).

Pressure drop across the substrates was evaluated by measuring the pressure upstream and downstream of the substrate, at mass flow rates from 50 to 500 kg/h. These correspond to a range of exhaust velocities from 5 to 25 m/s. The pressure was measured on the wall of the flow rig, several millimeters upstream and downstream of the substrate, assuming that the pressure distribution across the entire cross-section is uniform. This configuration helps to evaluate the effect of the pressure drop of the substrate alone, isolating it from the effect of the pressure drop of the inlet duct. For low mass flow rates, a Schiltknecht digital, capacitive manometer was used, with a range of 0–20 hPa for upstream measurements, and 0–10 hPa for downstream measurements. For higher mass flow rates, two analog manometers were used, with a range of 0–100 hPa.

## 2.2 Application of particle image velocimetry (PIV)

For the flow field analysis the 2-d PIV technique was chosen. 2-d PIV is nowadays a more or less a standard measuring technique. However, a PIV system is a complex measurement chain with a series of independent choices in hardware and software parameters influencing results as well as the associated resolution. The following description aims in highlighting the most interesting issues.

As a light source, two independent optically coupled, frequency doubled Nd:YAG-lasers were used. The beam followed an optical path mainly consisting of two cylindrical lenses (−75 and 1,000 mm focal lengths). Dried and filtered $TiO_2$ particles have been dispersed in the flow upstream of the inflow tube. The dispersion was carried out by a home-made solid-powder atomizer. The average particle aerodynamic diameter has been measured by an electrical low pressure impactor (ELPI) and was found to be around 700 nm. Further details of the instrument can be found in Keskinen et al. (1992). According to (Dimopoulos 1996) such particles can follow turbulent structures with frequencies up to 10 kHz with 90% accuracy. This was considered as sufficient given the limitations of the camera system used allowing a repetition rate for a double exposure acquisition of 3 Hz.

Perpendicular to the laser sheet, a $1,280 \times 1,024$ pixel CCD camera was mounted. The diameter of each CCD pixel was 6.7 µm. The camera lens had a 75-mm focal length, resulting in a magnification factor of 0.118, i.e., 56.8 µm/pixel. The lens had to satisfy two requirements; on the one hand, a large view field (in the order of the duct dimensions), and on the other hand, particle images in the order of a camera pixel size. A moderate f/5.6 aperture value was chosen, in order to have a good compromise between spatial and light filtering. The scattered light image of a particle is a function of the optical imaging properties as well as of its diffraction image. Using the relations given by (Herrmann 2002), the diffraction image of a particle associated with the used optics is around 8.2 µm, while the optical image of an average particle lies around 0.08 µm. Hence the resulting particle image is in the order of magnitude of a CCD camera pixel.

Processing of the flow images was performed with the cross-correlation method over discrete interrogation window areas. The optimal interrogation window size was a further investigation item and was found to be $32 \times 32$ pixels (Dimopoulos et al. 2007). In combination with a 50% overlap of the interrogation windows (and the optical imaging) one velocity vector per 0.908 mm was obtained. The chosen size of the interrogation window, ensuring the existence of 3–6 particles in each window, leads to appropriate velocity resolution and satisfied a flow continuity criterion with acceptable accuracy (Dimopoulos et al.

2007). It should be underlined that the interrogation window acts as a spatial averaging filter, integrating velocity information over its area ($0.908 \times 0.908$ mm$^2$). Table 1 summarizes the most important features of the PIV system employed. Given the velocity resolution values, as well as the expected flow velocities (Table 1), the chosen time $\Delta t$ between the two exposures may seem too short. It should be kept in mind though, that the flow was highly asymmetric, having higher velocities in one half of the duct. In the direct downstream of the catalyst substrates, where the flow is characterized by small scales, the interrogation window size may cause some distortion; in particular, in case where the interrogation spot lies partly in a pore outflow jet and partly in its wake.

## 2.3 Flow field evaluation

The evaluation of each double exposure resulted in the instantaneous flow field. For each measurement configuration around 1,500 double exposures have been captured and evaluated. The velocity vectors have been analyzed in the axial (longitudinal) and lateral (transversal) components according to the $x$ and $y$ directions in Fig. 1. The averaging of the velocity vectors at every location resulted in the average velocities while the standard deviation of all measured velocities from the average velocity was computed for characterizing the turbulence intensity at each location.

In order to quantify the homogeneity of the flow field we introduced the flow uniformity factor (UF) according to (Nagel and Diringer 2000),

$$ \text{UF} = 1 - \sqrt{\frac{1}{n}\sum_n \left(\frac{u_i - \bar{u}}{\bar{u}}\right)^2} \qquad (1) $$

where $u$ is the local exhaust gas velocity, and $\bar{u}$ is the average velocity of a flow profile. The expression is formulated in such a way that in the case of a completely uniform distribution, UF takes the maximum value of 1.

The UF is sometimes also called maldistribution factor (Stratakis and Stamatelos 2004), or $\gamma$-factor (Windmann et al. 2003).

## 2.4 Compared substrates

Four substrates were compared in the framework of this work: a conventional honeycomb monolith and three ceramic foam substrates with different pore densities. The honeycomb monolith had a cell density of 400 cpsi (cells per square inch), comprised of square cells of approx. 0.9 mm side length. The ceramic foams had 8, 10, and 15 ppi (pores per inch) densities, corresponding to 0.032, 0.016, and 0.0048 cm$^3$ mean pore volume, or 1.97, 1.58, and 1.05 mm pore radius, respectively. All substrates had a square cross-section of $75 \times 75$ mm$^2$, corresponding to a frontal area of 56 cm$^2$. This frontal area is rather small for typical passenger car substrates, which usually have frontal area in the order of 75–100 cm$^2$. The basic substrate length was 72 mm, while measurements with smaller substrate lengths have also been performed.

Foam samples are characterized by their pore diameters and open void fractions. The mean pore size was given by the ppi (pores per inch) specification of the organic foam basis. The open-void fraction, also called porosity, $\varepsilon$, is defined as the ratio between the accessible empty volume and the total volume. Since the accessible empty volume is not easily to be measured, the porosity estimation was based on the densities ratio:

$$ \varepsilon = 1 - \frac{\rho_{\text{foam}}}{\rho_{\text{struts}}} \qquad (2) $$

The foam densities $\rho_{\text{foam}}$, have been obtained by measuring the volume and the weight of a series of samples. The strut densities $\rho_{\text{struts}}$ have been measured by Helium pycnometry. Out of approx. 120 different manufactured and measured foams reasonably constant strut and foam densities have been obtained regardless of other foam parameters (mean pore seize etc.). Hence the

**Table 1** Parameters of the PIV set-up

| Magnification | 0.118 | | | | | |
|---|---|---|---|---|---|---|
| Pixel image | 56 μm | | | | | |
| Field of view | 56.56 mm 47.22 mm | | | | | |
| Interrogation window | $32 \times 32$ pixels | | | | | |
| Overlap | 50% | | | | | |
| Spatial Res. | $0.908 \times 0.908$ mm$^2$ | | | | | |
| Flow rate [kg/h] | 100 | 150 | 200 | 250 | 300 | 370 |
| Exposure sep. time [μs] | 18 | | 12 | | 9 | |
| Mean flow vel. [m/s] | 5.07 | 7.66 | 10.3 | 12.94 | 15.7 | 19.8 |
| Max. vel. by PIV [m/s] | 25.2 | | 37.85 | | 50.47 | |
| Min. vel. by PIV [m/s] | 0.044 | | 0.066 | | 0.087 | |

porosity was not affected by the mean pore size. The measured densities have been $\rho_{foam} = 363$ kg/m$^3$ and $\rho_{struts} = 3{,}920$ kg/m$^3$ resulting to a porosity of 91%.

## 3 Results and discussion

### 3.1 Pressure drop

For honeycomb monoliths, the main component of pressure drop is the viscous drag inside the substrate channels. Since the flow in the channels is in the laminar region, the law of Hagen–Poiseuille for pressure drop in channels with laminar flow is typically applied. This is a linear correlation of the exhaust gas mean velocity inside the channel:

$$\left(\frac{\Delta p}{L}\right)_{hon} = 32\mu \frac{u}{\varepsilon d_h} \tag{3}$$

where $\Delta p/L$ is the pressure drop per unit length, $\mu$ is the exhaust gas viscosity, $\varepsilon$ is the substrate porosity and $d_h$ is the channel hydraulic diameter. The hydraulic diameter of the square-shaped cells is equal to their side length, i.e., 0.9 mm. As shown in Fig. 2, this correlation predicts very accurately the measured pressure drop along the honeycomb monolith.

It is broadly accepted that the pressure drop in foams follows a quadratic correlation with the mean flow velocity, commonly referred to as the Dupuit equation or Forchheimer



**Fig. 2** Pressure drop per unit length across the 400 cpsi honeycomb monolith. *Dots* measured values; *Solid line* calculated by Hagen–Poiseuille correlation

equation, where the quadratic term accounts for the form drag around the ceramic foam struts:

$$\left(\frac{\Delta p}{L}\right)_{foam} = a_0 u + a_1 u^2 \tag{4}$$

Many researchers have tried to determine the coefficients $a_0$ and $a_1$ as a function of the fluid properties and the geometrical properties of the foam. A comprehensive review of the relevant literature was published recently by Edouard et al. (2008). In the simplest approach, Eq. 4 is written as a function of the fluid properties, i.e., viscosity $\mu$ and density $\rho$, and the substrate properties, i.e., permeability $K$ and form drag coefficient $C$ or $c_F$:

$$\left(\frac{\Delta p}{L}\right)_{foam} = \frac{\mu}{K}u + \rho C u^2 \text{ or } \left(\frac{\Delta p}{L}\right)_{foam} = \frac{\mu}{K}u + \rho\frac{c_F}{\sqrt{K}}u^2 \tag{5}$$

Then, the experimental pressure drop data are fitted to derive the values of the permeability and form drag coefficient (Boomsma and Poulikakos 2002; Dukhan 2006). Other approaches attempt to directly model the permeability and form drag coefficients, based on the geometrical properties of the foam. These approaches are usually based on the correlation proposed by (Ergun 1952) for the pressure drop through packed beds, which typically have porosities of 0.3–0.4:

$$\left(\frac{\Delta p}{L}\right)_{foam} = E_1 \frac{\mu(1-\varepsilon)^2}{\varepsilon^3 d_p^2}u + E_2 \frac{\rho(1-\varepsilon)}{\varepsilon^3 d_p}u^2 \tag{6}$$

where $d_p$ is the mean diameter of the particle in the packed bed and $E_1$ and $E_2$ are constants, with values 150 and 1.75, respectively. In order to predict the pressure drop through foams, which typically have a porosity of 0.85 or higher, researchers have applied geometrical models of the foam structure, to derive geometrical analogies with the packed beds (e.g., Innocentini et al. 1999; Richardson et al. 2000; Lacroix et al. 2007). These correlations can predict the pressure drop over a range of foam materials; however, most of them still require some constants to be fitted semi-empirically, in order to simulate a broader range of foam materials. The prediction of pressure drop becomes even more complicated by the fact that the pressure drop is sensitive to imperfections of the foam structure, which results in pressure drop variations for foams with similar apparent morphology (Incera Garrido et al. 2008).

In this context, we examine the pressure drop calculated by some of the proposed pressure drop correlations with the geometrical data of our foams and compare it to the measured pressure drop. Figure 3 presents this comparison for the 8, 10, and 15 ppi foams. For each substrate type, the pressure drop was measured with two substrate lengths. The correlations that we applied to calculate the pressure
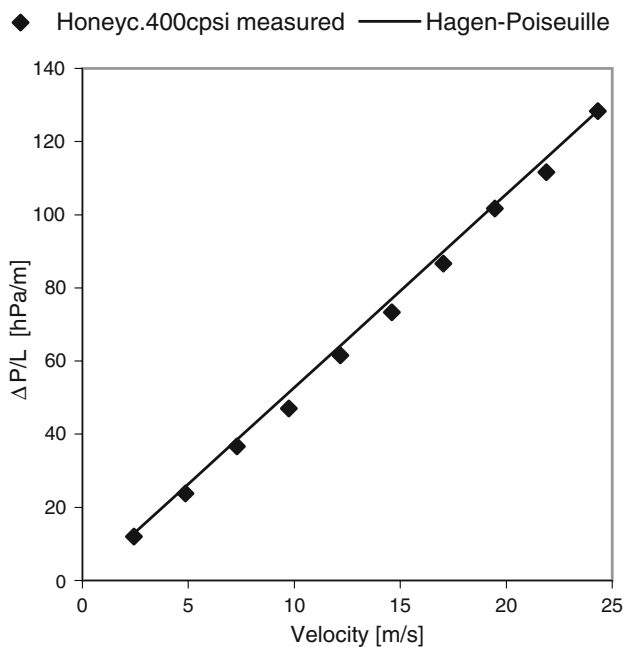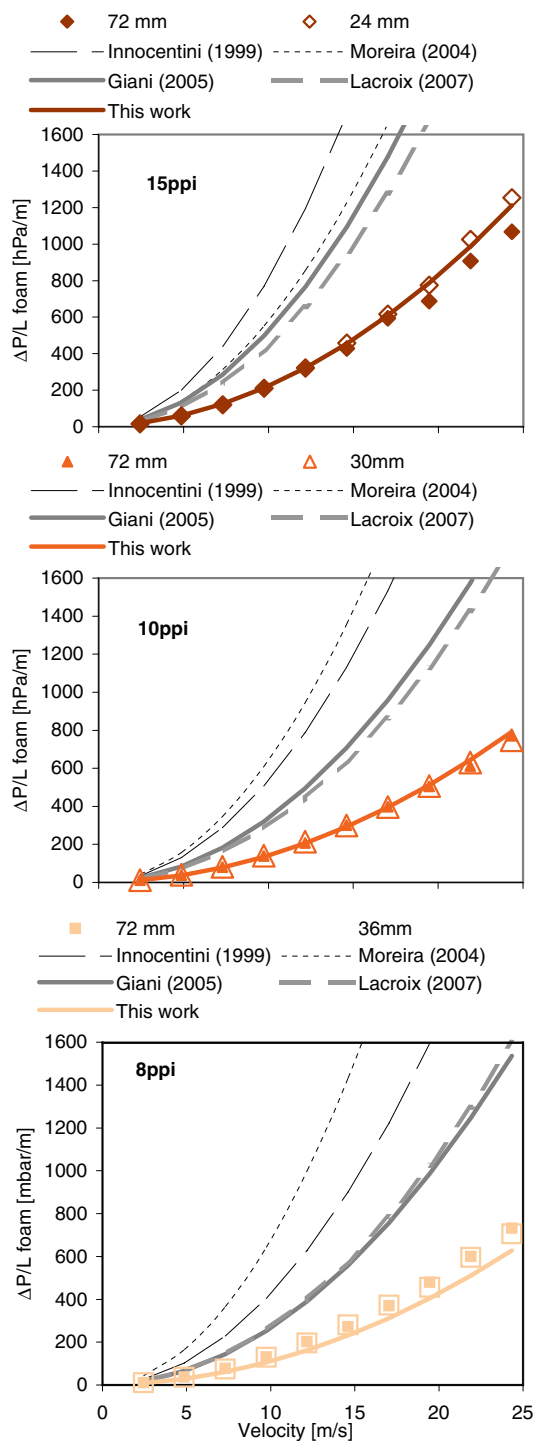
**Fig. 3** Pressure drop per unit length across the 15 ppi (*top*), 10 ppi (*middle*) and 8 ppi (*bottom*) ceramic foam monolith. *Dots* measured values; *Lines* calculated using different correlations

drop of the foam samples are summarized in Table 2. The strut diameter, $d_s$, was calculated based on a cubic cell model. The use of dodecahedron or tetrakaidekahedron cell models for calculation of $d_s$ resulted in less than 15% influence in the calculated pressure drop. The pore

diameter, $\alpha$, was calculated from the average pore volume, which was in turn calculated under the assumption of an isotropic foam with spherical pores. The correlation of (Giani et al. 2005) is based on a model of a bundle of tubes, with a friction factor fitted based on experimental data. The correlation of (Innocentini et al. 1999) uses the Ergun equation, based on an equivalent particle diameter, $d_p$, calculated by the geometrical properties of the foam. The correlation of (Lacroix et al. 2007) also uses the Ergun equation, but employs a different formula for calculating the equivalent particle diameter, $d_p$. The correlations of Giani and Lacroix predict similar pressure drop values. All correlations predict higher pressure drop values for our substrates, compared to the measured pressure drop. Therefore, we resorted to a correlation with semi-empirical fitted constants, aiming to have only one set of constants for all of the foam densities we tested. The best result we obtained was by using the correlation of Inoccentini, with modified constants. The correlation used is included in Table 2. The calculated pressure drop agrees quite well with the experiment, for the 10- and the 15-ppi foams. However, this is not the case for the 8-ppi foam, where the calculated pressure drop is lower. Interestingly, the difference between the pressure drop measured with the 8- and 10-ppi foam is very small. It could be the case that three-dimensional flow non-uniformities in the 8-ppi foam increase the overall pressure drop, to an extent where the 1-d correlation, including only the mean flow velocity, is not able to predict. Compressibility effects on the pressure drop correlation have not been examined in this context, due to the low Mach number (Mach <0.1). It is a common approach of most catalytic converter models to treat the flow as incompressible.

An overall comparison of the pressure drop of the tested substrates is plotted in Fig. 4. At the upper range of exhaust gas velocities, the pressure drop per unit length of the 10-ppi ceramic foam is 4–6 times higher than the pressure drop of the honeycomb monolith. The 15-ppi foam presents almost double pressure drop compared to the 10-ppi foam, which is almost an order of magnitude higher, compared to the honeycomb monolith.

These differences in the pressure drop per unit length between ceramic foams and honeycomb monoliths should be examined in the correct context though. First, foam substrates with shorter length can achieve the same conversion as longer honeycomb substrates (Giani et al. 2005); this means that if we examine the total pressure drop, and not the pressure drop per unit length, the differences between foams and honeycombs will be smaller. Second, the pressure drop is strongly affected by the gas temperature, given that increasing the temperature, reduces the gas density and increases flow velocity and gas viscosity. Therefore, in order to obtain a more realistic idea of the

**Table 2** Selected pressure drop correlations for ceramic foams

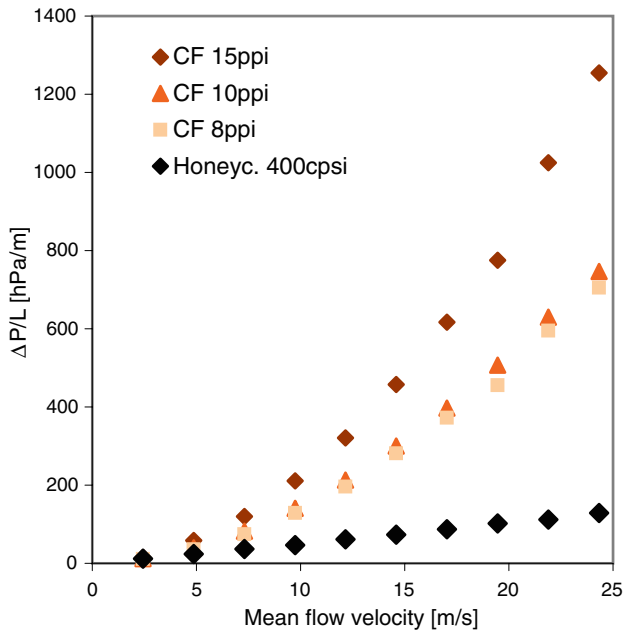| Authors | Pressure drop correlation | Characteristic properties |
| --- | --- | --- |
| Innocentini et al. (1999) | $\left(\frac{\Delta p}{L}\right)_{foam} = 150\frac{(1-\varepsilon)^2}{\varepsilon^3 d_p^2}\mu u + 1.75\frac{(1-\varepsilon)}{\varepsilon^3 d_p}\rho u^2$ | $d_p = 1.5a\frac{1-\varepsilon}{\varepsilon}$ |
| Moreira and Coury (2004) | $\left(\frac{\Delta p}{L}\right)_{foam} = 1.275\cdot 10^9\frac{(1-\varepsilon)^2}{\varepsilon^3 a^{-0.05}}\mu u + 1.89\cdot 10^4\frac{(1-\varepsilon)}{\varepsilon^3 a^{-0.25}}\rho u^2$ | |
| Giani et al. (2005) | $\left(\frac{\Delta p}{L}\right)_{foam} = 13.56\frac{1}{2ad_s(1-d_s/a)^4}\mu u + 0.87\frac{1}{2a(1-d_s/a)^4}\rho u^2$ | |
| Lacroix et al. (2007) | $\left(\frac{\Delta p}{L}\right)_{foam} = 150\frac{(1-\varepsilon)^2}{\varepsilon^3 d_p^2}\mu u + 1.75\frac{(1-\varepsilon)}{\varepsilon^3 d_p}\rho u^2$ | $d_p = 1.5d_s$ |
| This work | $\left(\frac{\Delta p}{L}\right)_{foam} = 150\frac{(1-\varepsilon)^2}{\varepsilon^3 d_p^2}\mu u + 0.43\frac{(1-\varepsilon)}{\varepsilon^3 d_p}\rho u^2$ | $d_p = 1.5a\frac{1-\varepsilon}{\varepsilon}$ |



**Fig. 4** Measured pressure drop per unit length across the different substrates tested



**Fig. 5** Pressure drop per unit length for substrates with a circular cross-section with 0.1 m diameter, calculated for ambient temperature (300 K) and a typical exhaust gas temperature (800 K)

pressure drop of the foam versus honeycomb substrates, we performed a comparison with realistic exhaust gas temperature and mass flow rate, as well as realistic substrate geometry. This comparison is illustrated in Fig. 5, where we plot the calculated pressure drop per unit length for the honeycomb substrate and the 10-ppi ceramic foam. The calculation is performed for the range of expected mass flow rates for a 2.0-l engine, assuming a substrate with circular cross-section and 0.1 m diameter, at two different temperatures: ambient temperature (300 K), and a representative exhaust gas temperature (800 K). However, as we have validated the pressure drop correlations only with cold-flow measurements, applying them to hot flow conditions may involve inaccuracies, particularly concerning the ceramic foams. A more systematic validation under cold-flow and hot-flow conditions, with washcoated and non-washcoated substrates is required. This investigation would also enable us to assess the pressure drop variability between foams with the same pore density.
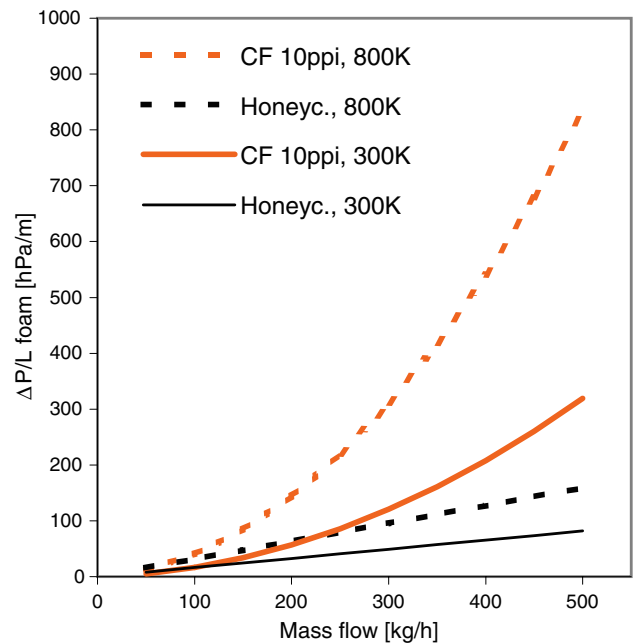
### 3.2 Flow field downstream of the substrate

The flow field downstream of the catalyst substrate is expected to present some fundamental differences between honeycomb monoliths and ceramic foams. Below, we investigate the differences in the mean flow velocity field, and in the turbulence intensity.

#### 3.2.1 Flow velocity field

The main difference between a honeycomb monolith substrate and a foam substrate in terms of flow velocity is that the honeycomb monolith does not allow any momentum exchange perpendicular to the main flow direction, while the foam, in principle, allows the exhaust gas to flow in all directions through it. The effects of this difference are illustrated in Fig. 6, which plots the flow field downstream
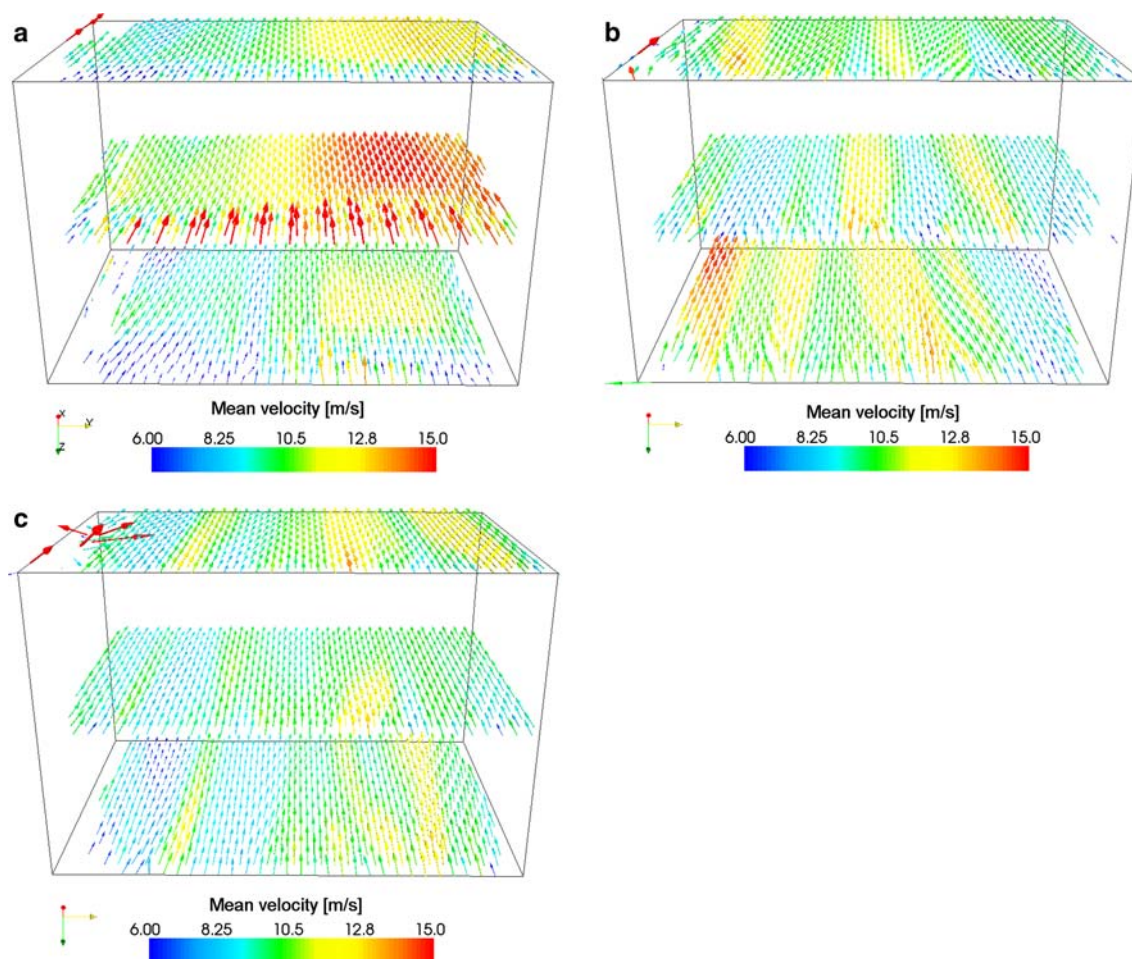
**Fig. 6** Vector plot of the velocity field downstream of the catalyst substrate. Substrate dimensions: $75 \times 75 \times 72$ mm$^3$. Mass flow rate: 250 kg/h. **a** Honeycomb monolith, 400 cpsi, **b** ceramic foam, 8 ppi, **c** ceramic foam, 10 ppi

of three different substrates of equal length (72 mm), for a mass flow rate of 250 kg/h. Figure 6a shows the flow velocity field downstream of a 400 cpsi honeycomb monolith. We may observe that the bulk flow is located at the right half of the duct. This is caused by the inlet duct geometry, conducting the larger part of the flow towards the right half of the substrate inlet (Fig. 1). This maldistribution is clearly observable even at the substrate outlet. Another interesting observation from Fig. 6a is the fact that the flow right after the monolith exit is unevenly distributed having distinctive local maxima and minima. These local minima and maxima are spaced by roughly 4.5 mm, and they do not resemble the monolith channel structure, which consists of 0.9 mm-wide channels with 0.165 mm-thick channel walls. Probably some "optical aliasing" effect through the PIV evaluation is involved, since the interrogation spot size of the PIV evaluation algorithm is 0.908 mm. Nevertheless, this flow pattern is surely associated with the accumulating free jet flows downstream of each monolith channel. The presence of these free jets is an interesting observation,

which cannot be reproduced by the commonly applied CFD simulation approach, which treats the monolithic substrate as a homogeneous porous medium.

Figure 6b presents the respective flow field downstream of an 8-ppi ceramic foam substrate. In contrast to the honeycomb monolith, the flow distribution here is better balanced. Neither the large-scale jet, caused by the geometry of the inlet duct, nor the small-scale jets, caused by the substrate channels can be observed. However, some intermediate-scale jets are present at various locations. These jets do not always point towards the axial direction, but some of them appear to point towards various transversal directions, and they are not large enough to be traced in more than one measurement plane. This implies that similar jets may exist between the planes that we measured, suggesting a highly three-dimensional flow pattern. This flow pattern could be attributed to local non-uniformities in the foam structure. In Fig. 6c, the respective velocity field downstream of a 10-ppi ceramic foam is presented. Compared to the 8-ppi ceramic foam, fewer jets are observed,

and the flow pattern appears to be more uniform. This could be a result of the increased cell density of the ceramic foam, or of a more uniform foam structure.

In the vicinity of the left side-boundaries of the duct, measurement quality decreases resulting also in several apparent artifacts. In this location, the laser sheets enter into the duct through the optical access window. The associated light scattering increases background noise, leading to low measurement validation and to a small number of obviously erroneous velocity vectors.

The uniformity of the flow fields can be more clearly illustrated by plotting the axial velocity profiles. In Fig. 7 we plot the mean axial velocity profiles 47 mm downstream of the substrate exit, at the median measurement plane, normalized against the average velocity of each profile. The mean axial velocities downstream of the ceramic foams present a generally uniform velocity profile, with local peaks corresponding to the intermediate-scale flow jets observed in Fig. 6. In contrast, the velocity profile of the honeycomb monolith is highly asymmetric, reflecting the asymmetry of the upstream flow prior to passing through the monolith. These velocity profiles suggest that the ceramic foam substrates tested have a significantly stronger homogenizing impact on the flow than the honeycomb monolith. For a clear display, we used continuous curves for the velocity profiles. It should be though kept in mind that the lines are consisting of discrete points having the mentioned 0.908 mm resolution.

Another way to quantify the flow uniformity is by the flow UF, as defined in Sect. 2.3. The UF of the velocity
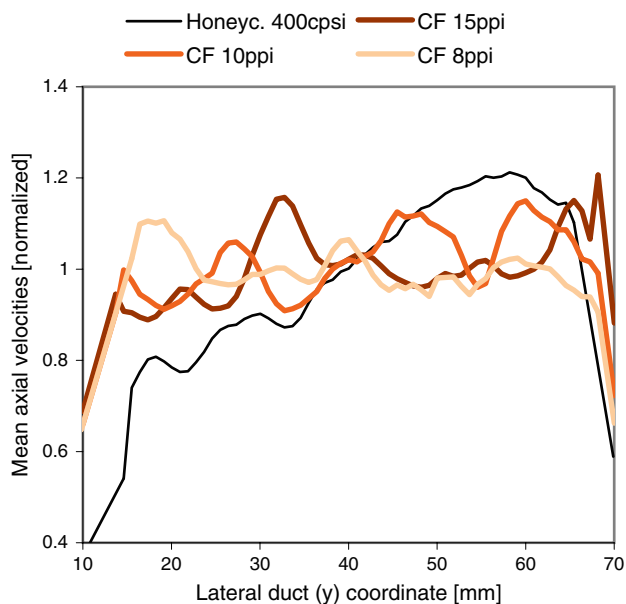


**Fig. 8** Evolution of the uniformity factor along the duct downstream of the substrate exit. Mass flow rate: 250 kg/h, median height of the duct



**Fig. 7** Normalized axial velocities 50 mm downstream the exit of the substrates. All substrates of identical outer dimensions $(75 \times 75 \times 72 \text{ mm}^3)$. Mass flow rate: 250 kg/h, median height of the duct
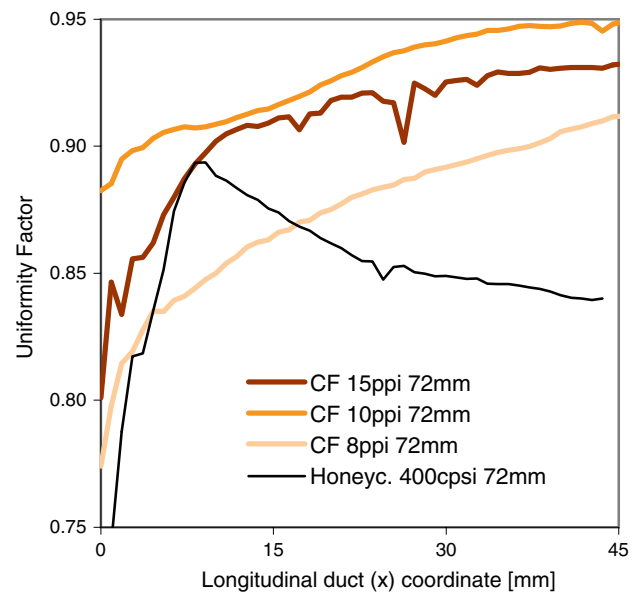
profiles on the median measurement plane is plotted in Fig. 8, as a function of the longitudinal duct coordinate, i.e., the distance from the exit of the substrate. We may observe that for all ceramic foams the flow becomes more uniform as the distance from the substrate exit increases. This is caused by the mixing of the intermediate-scale jets like the ones observed in the vector plots of Fig. 6. This trend does not appear in the case of the honeycomb monolith. Instead, the UF increases in the first 10 mm after the substrate exit, as a result of the mixing of the small-scale jets from the monolith channels, but afterwards the UF decreases almost asymptotically, as the flow uniformity becomes governed by the large-scale jet caused by the inlet duct geometry. This can also be observed in the vector plot of Fig. 6a, where the flow appears to be quite uniform at a distance of 10–15 mm downstream of the substrate; but at a higher distance, the large-scale jet becomes clearly visible. We cannot be sure to what extent this behavior of the UF is affected by the inaccuracies of the measurement of the small-scale jets downstream of each monolith channel. However, we can be confident that the asymptotic value 50 mm downstream of the substrate is correctly captured. Comparing this value with the respective values for the ceramic foams, we notice that all ceramic foams appear to achieve better flow uniformity than the honeycomb monolith, and the 10-ppi foam appears to achieve the best flow uniformity.

### 3.2.2 Turbulence intensity

The measured turbulence intensities downstream of three different substrates are illustrated in Fig. 9. In all cases,

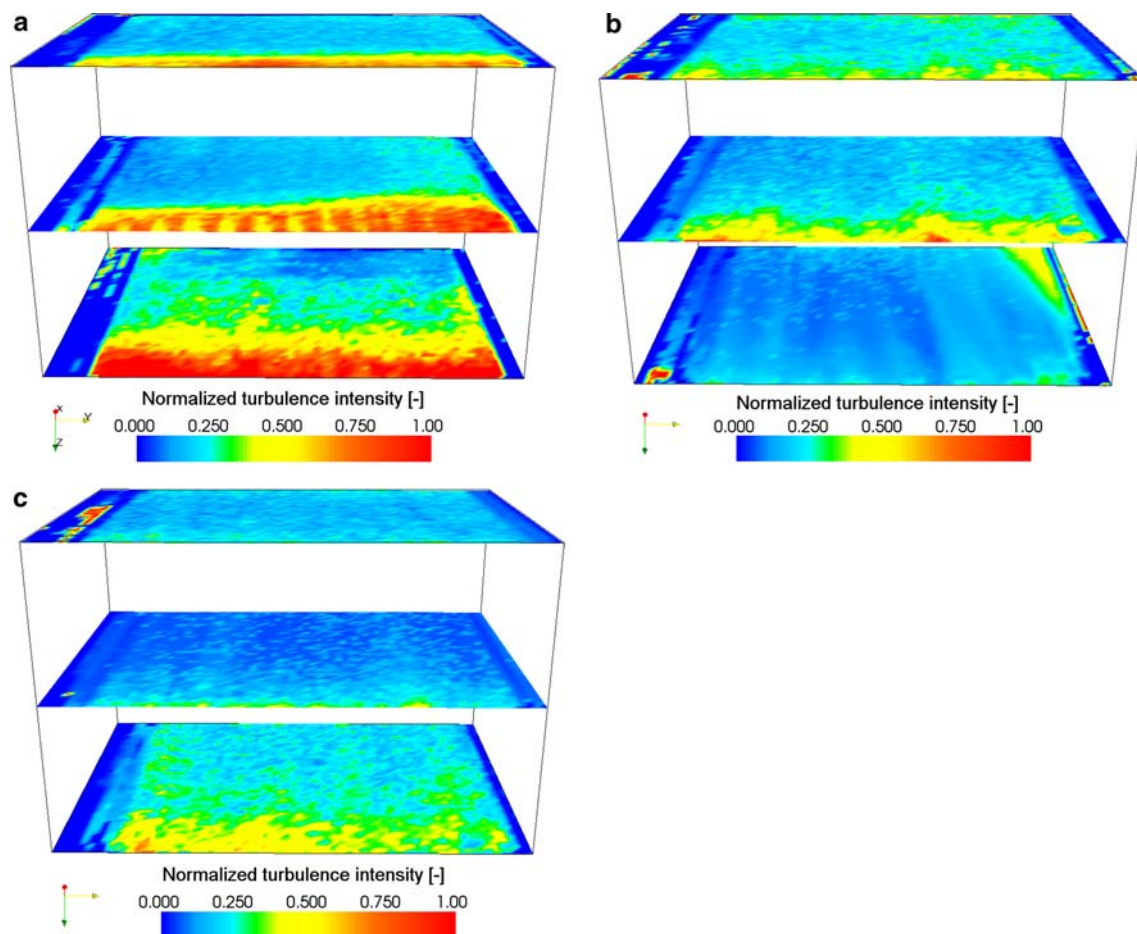**Fig. 9** Contour plots of the measured turbulence intensity field downstream of the substrates. Substrate dimensions (75 × 75 × 72 mm$^3$). Mass flow rate: 250 kg/h. **a** Honeycomb monolith, 400 cpsi, **b** ceramic foam, 10 ppi, **c** ceramic foam, 8 ppi

some artifacts appear, especially near the boundaries of the measurement field, due to the interpolation procedure between several points, where the PIV measurement has high uncertainty. Very high levels of turbulence, reaching turbulence intensities up to 0.8 or even higher, can be observed in the first 15 mm downstream of the honeycomb monolith substrate. Interestingly, this region of high turbulence intensity extends through the entire monolith width, in all measurement heights. This region can be attributed to the formation of the small-scale free jets downstream of the individual monolith channels. It should be kept in mind though, that the PIV-optics resolution of 0.908 mm, contributes to some extent to a feigned increase of turbulence values. Given that the small-scale free jets are smaller than the integration area (of the PIV interrogation spots) velocity information is averaged over free jet and boundary recirculation areas, leading thus to some degree of deceiving turbulence enhancement. Future steps will investigate the flow field with a higher optical resolution, aiming to address these issues. The advantage of better small-scale resolution, though, will be

counterbalanced by loss of the large scale flow information presented here.

Such high levels of turbulence intensity are not observed downstream of the ceramic foams. On the one hand, the higher flow uniformity dampens turbulence fluctuations, and on the other hand the bigger size of the small-scale jets reduces apparent turbulence amplification through the PIV system. However, the turbulence intensity again appears to be higher directly after the substrate, but this does not happen consistently for all measurement planes. In the 8-ppi foam the median and lower measurement heights appear to be more turbulent, while the opposite is the case with the 10-ppi foam. At locations further downstream in the measurement field, no significant differences in the turbulence intensity appear to exist between the three substrates examined.

### 3.2.3 Linking between pressure drop and flow uniformity

The previous results show that the flow distribution downstream of the ceramic foams is more uniform compared

to the honeycomb monolith. This higher uniformity should be carefully interpreted though as the ceramic foams have significantly higher pressure drop per unit length than the honeycomb monolith. It is well known and has been previously demonstrated that the flow uniformity increases when the pressure drop across the substrate increases. Therefore, it is important to view the flow uniformity downstream of each substrate in relation to the substrate pressure drop. Models correlating the pressure drop of honeycomb monoliths with the flow uniformity in the case of simple 2-d flow patterns have been presented (e.g., Tsinoglou et al. 2004). A similar correlation for the complex 3-d flow patterns observed here is not possible with the data gathered in the framework of this study. However, we may examine the correlation between pressure drop and flow uniformity in a qualitative way.

First, we compare the velocity profiles downstream of different substrates having similar pressure drop values. In order to achieve similar pressure drop for the ceramic foams and the honeycomb monolith, we used foams with smaller length, namely 36 mm for the 8-ppi foam and 24 mm for the 15-ppi foam. The above substrates have comparable pressure drop at exhaust velocities up to 12 m/s, which corresponds to a mass flow rate of 250 kg/h. The comparison of the velocity profiles is performed in Fig. 10, which shows the mean axial velocities at the median measurement plane, 50 mm downstream of the substrate exit. The velocity profiles of the shorter ceramic foams are less uniform than the ones of the longer foams depicted in Fig. 7,

and the effect of the flow non-uniformity imposed by the inlet duct geometry is now visible downstream of the ceramic foams. But still the velocity profiles downstream of the ceramic foams are more uniform than the respective profile of the honeycomb monolith.

Second, we shall examine the effect of the exhaust gas velocity on the flow uniformity. In Fig. 11, the normalized velocity profiles 50 mm downstream of two different substrates are plotted, for two different mass flow rates. In the case of the honeycomb monolith, the velocity profile for the high mass flow rate is clearly less uniform, compared to the low mass flow rate. The observation that the flow uniformity in honeycomb monoliths decreases, with increasing mass flow, has been well-documented in the literature (Wendland and Matthes 1986). This trend is not observed in the case of the 10-ppi ceramic foam though, where the differences in the normalized velocity profile between the low and the high mass flow rate, are small. This effect is further quantified in Fig. 12, where the flow UF 50 mm downstream of the substrate exit, at the median measurement plane, is plotted against the exhaust gas velocity. The flow uniformity of the honeycomb monolith decreases with increasing exhaust gas velocity, as expected. The flow uniformity of all ceramic foams though, is practically unaffected by the mass flow rate. A possible explanation could be found again in the increased pressure drop; the pressure drop of honeycomb monoliths increases linearly with exhaust gas velocity, while the pressure drop of ceramic foams increases by a quadratic expression. As a result, the high pressure drop of ceramic foams at high
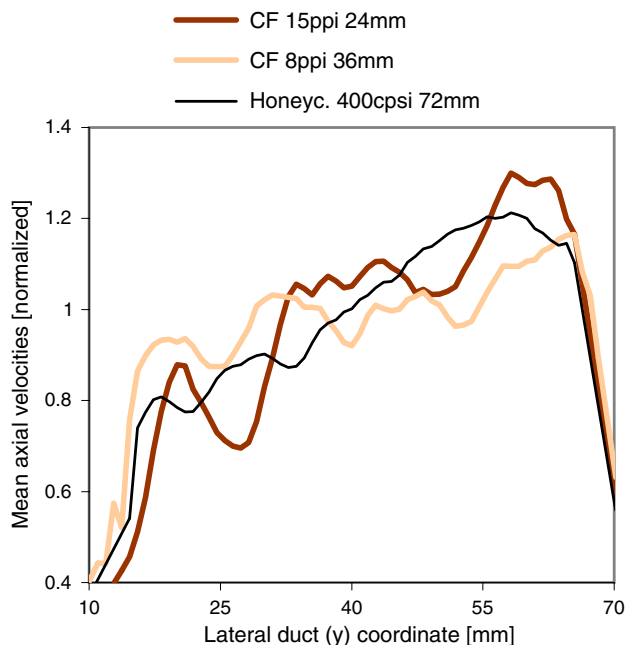


Fig. 10 Normalized axial velocities 50 mm downstream of the substrate exit. Substrate dimensions chosen for similar pressure drop. Mass flow rate: 250 kg/h, median height of the duct
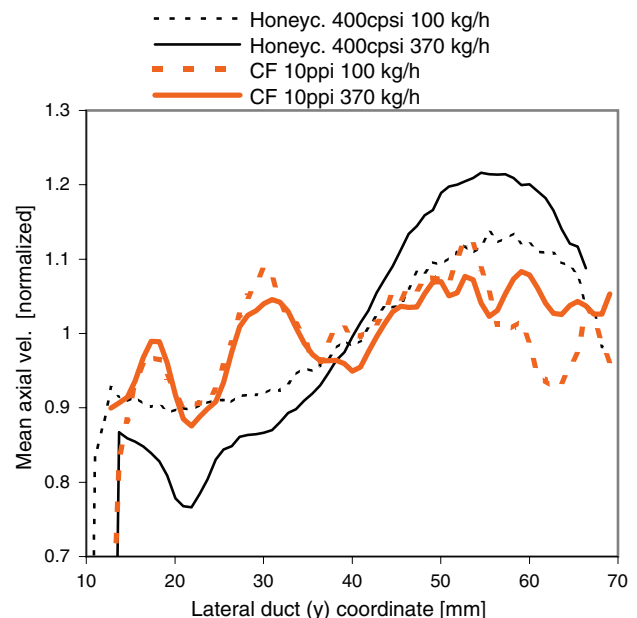


Fig. 11 Normalized axial velocities 50 mm downstream of the exit of the substrates. Effect of mass flow rate. 400 cpsi honeycomb monolith and 10 ppi ceramic foam, median height of the duct
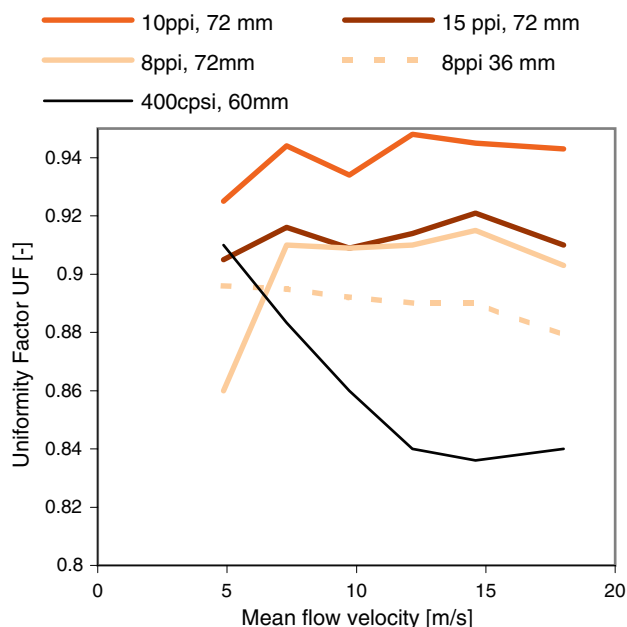
**Fig. 12** Flow uniformity factor at the median height of the duct as a function of mass flow rate, for different substrates

mass flow rates could prevent the increase of flow non-uniformity.

To examine if the increased flow uniformity of the ceramic foam is primarily caused by the increased pressure drop, or if it is a result of the substrate structure, which allows transversal gas flow, we shall compare the velocity distribution upstream and downstream of the substrate. This comparison is illustrated in Fig. 13. In the case of the empty
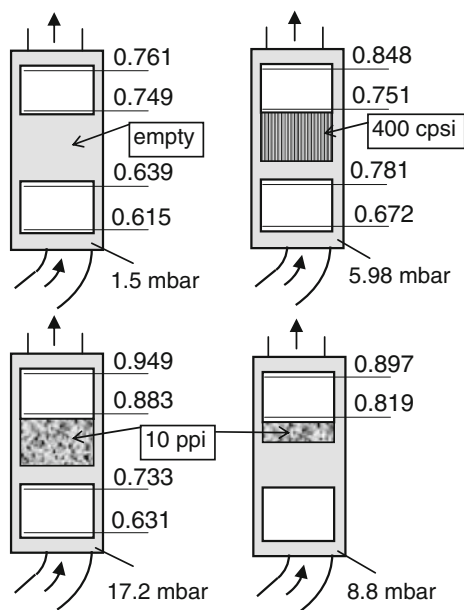


**Fig. 13** Schematic of the evolution of the uniformity factor along the duct downstream of the substrate exit. Different substrates, mean flow of 250 kg/h, median height of the duct

duct, the flow upstream of the substrate position has a UF = 0.639, while the flow at the furthest downstream position has a UF = 0.761, indicating that the initial flow non-uniformity caused by the inlet duct geometry is gradually dampened inside the duct. When a honeycomb monolith is placed in the substrate position, the flow becomes more uniform, both upstream and downstream of the substrate, as a result of the pressure drop imposed by the substrate. As expected, the velocity distribution upstream and downstream of the monolith is very similar, as no flow perpendicular to the main flow axis is possible inside the substrate. The situation is reflected by the UFs upstream and downstream of the monolith. The monolith increases the upstream flow uniformity to values of 0.672, 47 mm before the monolith entrance and to 0.781 directly before the monolith entrance. Directly after the monolith exit the flow uniformity is slightly lower, as a consequence of the micro jets generated by the gas exiting the channels.

On the contrary, the impact of ceramic foam substrates on the flow follows a different mechanism. The uniformity upstream of the ceramic foams is lower compared to the honeycomb monoliths, but as shown in Fig. 13, the uniformity downstream of the ceramic foams is higher. This finding provides evidence that a substantial part of the homogenizing impact of the ceramic foams is due to the internal structure of the foam, and the momentum exchange perpendicular to the main flow direction, and is not only due to the increased pressure drop imposed by the substrate structure.

## 4 Conclusions

Various applications of ceramic foams as catalyst substrates have been presented in the literature, mainly as alternatives to packed bed reactors used in industrial processes. For the application of ceramic foams as automotive catalyst substrates, several aspects of the substrate performance need to be further investigated. This paper presents an experimental investigation of the fluid dynamics aspects of ceramic foam substrates, compared to the widely used honeycomb monolith substrates.

The first aspect investigated is the pressure drop across the substrate. Previous studies suggest that the pressure drop through honeycomb monoliths follows a linear relationship, which can be described by the Hagen–Poiseuille equation, and that the pressure drop through ceramic foams is a quadratic function of the flow velocity. Our study confirmed the above, and showed that pressure drop correlations proposed in the literature cannot be directly applied to calculate the pressure drop across the foam samples tested. Therefore, a modified version of the Ergun equation was proposed based on similar approaches from the literature. The proposed correlation can capture the pressure drop at ceramic foams

with three different pore densities with the same parameterization. The experiments performed at ambient temperatures show that the ceramic foams involve higher pressure drops compared to honeycomb monoliths, particularly at high mass flow rates. Pressure drop calculations, using the proposed correlations, show that this difference is expected to be smaller at realistic exhaust gas temperatures.

The second aspect investigated was the effect of the substrate on the flow uniformity. Previous experimental and computational studies supported that the flow distribution directly upstream and downstream of honeycomb substrates is the same, as no momentum exchange perpendicular to the main flow occurs in the monolith channels. The PIV flow field investigations performed in the framework of this study showed that the flow field downstream of the honeycomb monoliths appears to be significantly affected by the individual flow jets downstream of each monolith channel. Our study confirmed previous studies suggesting that the flow downstream of honeycomb monoliths becomes less uniform with increasing mean flow velocity, but demonstrated that this is not the case with ceramic foam substrates, where the flow uniformity is practically not affected by the mean flow velocity. Moreover, ceramic foam substrates result in higher flow uniformity compared to honeycomb monoliths. The best flow uniformity was achieved downstream of 10 ppi foams. Foams with higher pore size (8 ppi) resulted in less uniform velocity profiles, while smaller pore size (15 ppi) increased pressure drop without improving flow uniformity.

These two flow dynamic aspects are closely linked to each other, according to several previous works, which demonstrate that increased substrate pressure drop results in increased flow uniformity. By comparing the velocity profiles upstream and downstream of the substrates, we showed that the flow upstream and downstream of the honeycomb substrate was similarly uniform, but the flow downstream of the ceramic foams was significantly more uniform than the flow upstream. This finding suggests that the flow uniformity increases inside the ceramic foam, as a result of the momentum transfer perpendicular to the direction of the main flow, and not only as a result of the increased pressure drop.

# References

Boomsma K, Poulikakos D (2002) The effects of compression and pore size variations on the liquid flow characteristics in metal foams. J Fluids Eng 124(1):263–272

Chakravarthy VK, Conklin JC, Daw CS, D'Azevedo EF (2003) Multi-dimensional simulations of cold-start transients in a catalytic converter under steady inflow conditions. Appl Catal A 241:289–306

Dimopoulos P (1996) Experimentelle Untersuchung des Strömungsfeldes in motorischen Brennräumen. Ph.D. thesis, ETHZ Zurich

Dimopoulos P, Bach C (2008) Ceramic foams for automotive catalyst substrate applications, EET-European Ele-Drive conference, Geneva

Dimopoulos P, Bach C, Vogt UF, Herrmann K (2007) Ceramic foams as catalyst substrates: pre-catalyst application homogenising the exhaust flow upstream of aftertreatment devices. SAE 2007-24-0097

Dimopoulos P, Thurnheer T, Bach C (2008) High efficiency exhaust aftertreatment: purposeful application of ceramic foams, MTZ, Motorentechnische Zeitschrift, Conference "Der Antrieb von morgen", Munich, Germany

Dukhan N (2006) Correlations for the pressure drop for flow through metal foam. Exp Fluids 41(4):665–672

Edouard D, Lacroix M, Huu C, Luck F (2008) Pressure drop modeling on solid foam: state-of-the art correlation. Chem Eng J. doi:10.1016/j.cej.2008.06.007

Ergun S (1952) Fluid flow through packed columns. Chem Eng Prog 48(2):89–94

Gaiser G, Oesterle J, Braun J, Zacke P (2003) The progressive spin inlet-homogeneous flow distributions under stringent conditions. SAE Paper 2003-01-0840

Giani L, Groppi G, Tronconi E (2005) Mass-transfer characterization of metallic foams as supports for structured catalysts. Ind Eng Chem Res 44:4993–5002

Herrmann K (2002) Strömung, Flammencharakterisierung und Stickoxid-Bildung in turbulenten Vormischflammen. Ph.D. thesis, ETH Zürich

Hossfeld C, Ranalli M (2006) Katalysatorkonzept zur Reduzierung des Dieselpartikelfilter Volumens. MTZ 67:628–635

Incera Garrido G, Patkas FC, Lang S, Kraushaar-Czarnetzki B (2008) Mass transfer and pressure drop in ceramic foams: a description for different pore sizes and porosities. doi:10.1016/j.ces.2008.06.015

Innocentini MDM, Salvini VR, Macebo A, Pandolfelli VC (1999) Prediction of ceramic foams permeability using Ergun's equation. Mater Res 2(4):283–289

Kaiser R, Rusch K (2007) Auslegung von SCR-Systemen zur Stickoxidreduktion bei Dieselmotoren. MTZ 68:1062–1070

Keskinen J, Pietarinen K, Lehtimäki M (1992) Electrical low pressure impactor. J Aerosol Sci 23:353–360

Koltsakis GC, Katsaounis D, Samaras ZC, Naumann D, Saberi S, Böhm A (2006) filtration and regeneration performance of a catalyzed metal foam particulate filter. SAE 2006-01-1524

Koltsakis GC, Katsaounis D, Samaras ZC, Naumann D, Saberi S, Böhm A, Markomanolakis I (2008) Development of metal foam based aftertreatment on a diesel passenger car. SAE Paper 2008-01-0619

Lacroix M, Nguyen P, Schweich D, Huu CP, Savin-Poncet S, Edouard D (2007) Pressure drop measurements and modeling on SiC foams. Chem Eng Sci 62(12):3259–3267

Martin AP, Will NS, Bordet A, Cornet P, Gondoin C, Mouton X (1998) Effect of flow distribution on emissions performance of catalytic converters. SAE Paper 980936

Moreira E, Coury J (2004) The influence of structural parameters on the permeability of ceramic foams. Braz J Chem Eng 21(1):23–33

Nagel T, Diringer J (2000) Minimum test requirements for high cell-density, ultra-thin wall catalyst supports. SAE 2000-01-0495

Oesterle J, Gaiser G, Zacke P (2004) Homogeneous loading and regeneration of diesel particulate filters using progressive spin elements. SAE 2004-01-1424

Ranalli M, Hossfeld C, Keiser R, Schmidt S, Elfinger G (2002) Soot loading distribution as a key factor for a reliable DPF system. SAE 2002-01-2158

Richardson JT, Peng Y, Remue D (2000) Properties of ceramic foam catalyst supports: pressure drop. Appl Catal A: Gen 204(1):19–32

Stratakis GA, Stamatelos AM (2004) Flow maldistribution measurements in wall-flow diesel filters. IMechE Part D 218

Tsinoglou DN, Koltsakis GC, Missirlis DK, Yakinthos KJ (2004) Modelling of flow distribution during catalytic converter light-off. Int J Veh Des 34(3):231–259

Twigg M, Richardson J (2002) Theory and applications of ceramic foam catalysts. Chem Eng Res Des 80(2):183–189

Wendland DW, Matthes WR (1986) Visualization of automotive catalytic converter internal flows. SAE Paper 861554

Windmann J, Braun J, Zacke P, Tischler S, Deutschmann O, Warnatz J (2003) Impact of the inlet flow distribution on the light-off behavior of a 3-way catalytic converter. SAE 2003-01-0937

Zygourakis KT (1989) Transient operation of monolithic catalytic converters: a two-dimensional reactor model and the effects of radial nonuniform flow distribution. Chem Eng Sci 44(9):2075–2086